Marine and Petroleum Geology 26 (2009) 753–763

Contents lists available at ScienceDirect

Marine and Petroleum Geology

journal homepage: www.elsevier.com/locate/marpetgeo

Mesogenetic dissolution of the middle Ordovician limestone in the Tahe oilfield of Tarim basin, NW China

Zhijun Jin [a], Dongya Zhu [a,*], Wenxuan Hu [b], Xuefeng Zhang [b], Juntao Zhang [b], Yucai Song [b]

[a] Exploration and Production Research Institute of SINOPEC, Xueyuan Road #31, Haidian District, Beijing 100083, PR China
[b] Department of Earth Sciences, Nanjing University, Nanjing 210093, PR China

ARTICLE INFO

Article history:
Received 26 November 2007
Received in revised form 15 July 2008
Accepted 6 August 2008
Available online 22 August 2008

Keywords:
Limestone
Mesogenetic dissolution
Tarim basin
Trace element
Isotope

ABSTRACT

The mesogenetic dissolution is well developed in the middle Ordovician Yijianfang formation (O_2yj) limestone, and the dissolution pores are very important for petroleum accumulation in the south slope area of the Tahe oilfield which lies in the north of the Tarim basin, northwestern China. Mottled, dotted or laminar dissolution can be observed in the O_2yj limestone. Under microscope, the grains, lime matrix and all stages of calcite cements (including oil-inclusion-bearing blocky calcite cements) can all be found dissolved ubiquitously. The stylolites in the limestone were enlarged and rounded because of dissolution. Some dolomite rhombs, precipitated along stylolites in burial environment, were found dissolved as well. The dissolution of the blocky calcite cements and dolomite rhombs and the enlarging of stylolites demonstrate that the dissolution took place in the mesogenetic environment. Concentration of trace elements, including REEs, of the eroded part of the O_2yj limestone is intermediate between that of the uneroded part and that of the underlying lower Ordovician limestone hydrocarbon source rocks. Both $\delta^{13}C_{PDB}$ and $\delta^{18}O_{PDB}$ values of the eroded part are less than those of the uneroded part, respectively. The geochemical characteristics indicate that the eroding fluids are hydrocarbon-bearing fluids coming from the underlying hydrocarbon source rocks.

1. Introduction

Carbonates, in which about one-third of world's petroleum are preserved, are very important petroleum reservoir rocks throughout the world (Zenger et al., 1980). In the Tarim basin of Northwest China, the Ordovician carbonates are also one of the most important petroleum reservoir rocks. For example, the petroleum reserve in the Ordovician carbonates of the Tahe oilfield in the northern Tarim basin is more than 4.9 billion barrels.

Massive carbonate sediments deposited on shallow marine platforms or ramps generally have remarkably high primary porosity, up to 60–80% (Scholle, 1977). By the time such carbonate rocks are buried several hundreds to thousands of meters, they are mineralogically stabilized and their high depositional porosity and permeability are commonly reduced by intensive cementation and/or compaction (Halley and Schmoker, 1983; Scholle and Halley, 1985; Heydari, 1997). Therefore, the secondary dissolution porosity is considered to be critical for most carbonates to become efficient hydrocarbon reservoirs. Prior to the early 1970s, many geologists believed that major dissolution pores were formed mainly in subaerial meteoric environments (James and Choquette, 1984). Soon thereafter, however, as carbonate diagenesis in the mesogenetic environments (also referred to as deep-burial environments) was studied further, geologists not only found the existence, but also realized the significance, of dissolution pores developed in mesogenetic environments.

The find of mesogenetic dissolution, also called burial dissolution (Wang et al., 2003; Qian et al., 2007), deep dissolution (Ye et al., 1994), deep karst (Jia and Hao, 1989) and tectonic karst (Liu, 1997), was a great advance in studies of carbonate diagenesis in 1980s. It not only provides an important conceptual framework for hydrocarbon exploration in carbonate rocks but also points out a promising exploration prospect especially for the carbonates that have not yet suffered subaerial meteoric dissolution. Some characteristics of mesogenetic dissolution were discussed in detail by Mazzullo and Harris (1992). The fluid responsible for such dissolution was theoretically inferred to be the hydrocarbon-bearing fluid, which generally contains CO_2, H_2S and organic acids associated with diagenesis of organic matter in hydrocarbon source rocks. However, there are still no direct evidences to prove whether the aggressive fluid is exactly associated with diagenesis of organic matter in the hydrocarbon source rocks.

The mesogenetic dissolution of the Ordovician limestones in the Tarim basin had been discerned by many researchers, and the pores related to the mesogenetic dissolution had been proved to be an

* Corresponding author. Tel.: +86 108 228 2433.
E-mail address: zhudy@pepris.com (D. Zhu).

0264-8172/$ – see front matter © 2008 Elsevier Ltd. All rights reserved.
doi:10.1016/j.marpetgeo.2008.08.005

important reserving space (Zhang et al., 2004; Wang et al., 2003; Qian et al., 2006, 2007). The middle Ordovician Yijianfang formation (O_2yj) limestone of the Tahe oilfield in the north of Tarim basin has been proved to be one of the most prolific strata. The numerous tiny mesogenetic dissolution pores are discovered to contribute to almost all proportion of the reservoir space. In this paper, we start with a detail description of the characteristic of the mesogenetic dissolution, and then provide trace element and carbon and oxygen isotope evidences to determine the type of fluid for such dissolution.

2. Geological settings

The Tarim basin, in the northwest China, can be divided into seven principal structural units (Fig. 1), comprising three uplifts (Tabei (North Tarim), Central and Southeast Uplift) and four depressions (Kuche, North, Southwest and Southeast Depression) (Tong, 1992; Zhou and Zheng, 1990; Wang et al., 1992). The Tabei uplift is located in the north of the Tarim basin (Fig. 1). The Tahe oilfield lies in the south of Tabei uplift and borders upon Manjiaer sag to the southeast and Awati sag to the southwest.

A 6500–9500 m sedimentary sequence, comprising Cambrian to Tertiary strata, rests on Archaean and Proterozoic crystalline basement (Yung and Liu, 1992; Zhang, 1992). The Cambrian stratum mainly consists of tidal, platform and platform-margin marls, mudstones and carbonates/evaporates. The overlying lower Ordovician is primarily composed of platform dolomite and argillaceous limestone, while the middle-upper Ordovician mainly consists of platform and marginal slope-shelf carbonate sediments (Kang and Kang, 1996; Wei et al., 2000). The middle-upper Ordovician stratum can be subdivided into four formations, which are the Yijianfang (O_2yj), Qiaerbake (O_3q), Lianglitage (O_3l) and Sangtamu (O_3s) formations from bottom to top. The O_2yj formation consists mainly of wackestone, bioclast packstone and intraclast packstone. The O_3q and O_3l formations are composed mainly of micrite limestone with thin clay interlayers. The O_3s formation consists mainly of siliciclastic mudstone and sandstone.

The black/dark-gray Cambrian and lower Ordovician mudstones and mud-rich limestones in the Tarim basin, especially in Manjiaer sag, have long been considered to be source rocks (Lee, 1985; Fan et al., 1991; Graham et al., 1990; Wang et al., 1992; Hendrix et al., 1995; Zhang et al., 2000) for the hydrocarbons accumulated in the Ordovician reservoirs.

It has been well documented that the Ordovician carbonates in the Tahe oilfield were predominately altered by two periods of orogeny in middle–late Caledonia and early Hercynian, respectively. The two periods of orogeny controlled the characteristics of subaerial karstification of the Ordovician carbonates (Yu and Fu, 2006; Huang et al., 2006; Yan, 2002). Affected by the middle–late Caledonia orogeny, the north of the Tahe oilfield was uplifted and exposed at ground surface, and subsequently the Ordovician carbonates were severely eroded by meteoric water. In the early Hercynian orogeny, the north of the Tahe oilfield was uplifted again and the subaerial erosion was further strengthened. The former exposure resulted in an unconformity between the Silurian and Ordovician (S/O_1 in the north uplift, or S/O_3 in the south slope), and the latter resulted in another unconformity between Carboniferous (or Silurian) and early Ordovician (C/O_1 or S/O_1) in the north of the Tahe oilfield (Fig. 2).

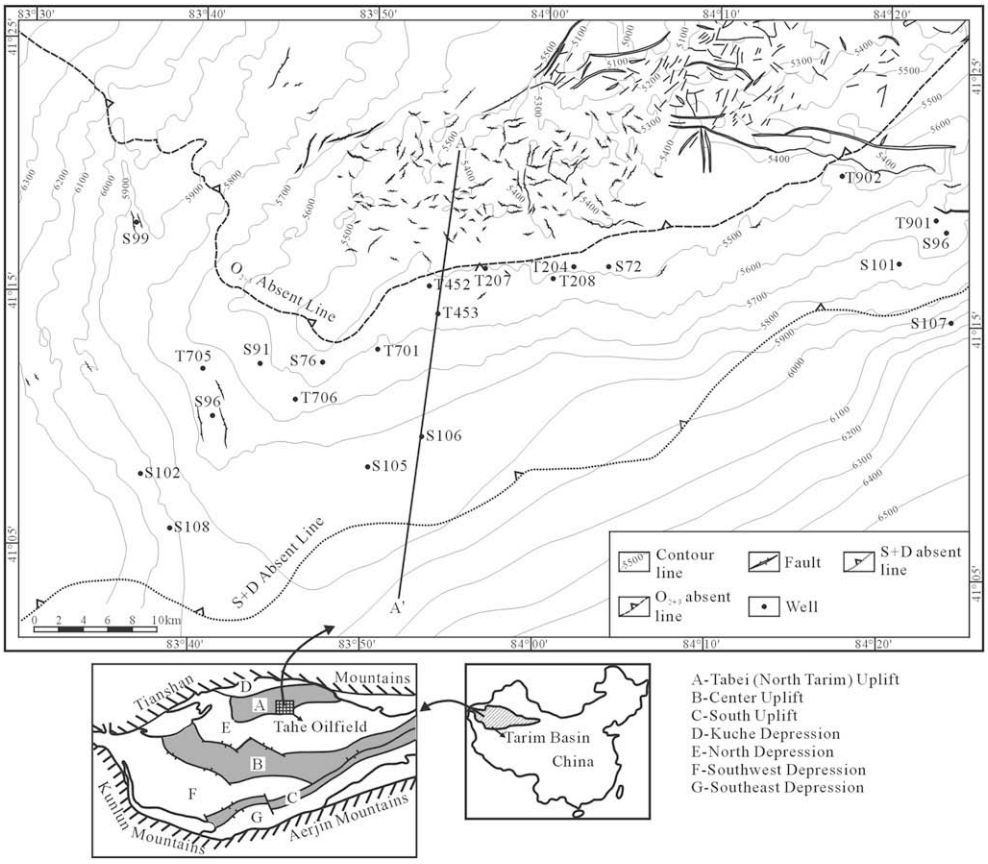

Fig. 1. Structures and wells with mesogenetic dissolution and industrial oil/gas flow in the Tahe oilfield. As implied by the contour map of the depth of the top of the Lower Ordovician, the geometry of the Paleozoic uplift is higher in the north and lower in the south. To the north of O_{2+3} absent line, all the O_{2+3} and party of O_1 carbonates were eroded by meteoric waters when they were exposed, leaving numerous large dissolution caves as reservoir spaces in the O_1 carbonates. Whereas to the south of the O_{2+3} absent line, the O_2yj limestone at the bottom of the O_{2+3} stratum was not eroded by meteoric waters. The mesogenetic dissolution was not only especially remarkable but also very important for hydrocarbon accumulation. The wells in this figure gave industrial oil/gas flow from the O_2yj limestone, which has substantial mesogenetic dissolution pores.

In the north uplift (to the north of the O_{2+3} absent line; Fig. 1), the middle-upper Ordovician strata were completely removed and the lower Ordovician carbonates were strongly subaerially eroded. The reservoir space in the lower Ordovician carbonates is mainly the pore and cavity system associated with subaerial meteoric erosion (Fig. 2). In contrast, as discovered by boreholes and seismic profiles, the middle Ordovician Yijianfang formation (O_2yj) limestone in the south slope area (to the south of the O_{2+3} absent line; Fig. 1), had never been subaerially exposed and subsequently had not been altered by meteoric water because it was buried well below the two unconformities (Fig. 2) and beyond the reach of meteoric water. Therefore, the reservoir space in the O_2yj limestone in the south slope is dominantly mesogenetic dissolution pores (Fig. 2). Many wells in the south slope area produce industrial oil/gas flow from mesogenetic dissolution pores in the O_2yj limestone.

3. Samples and methods

About 100 core samples of O_2yj limestone were collected from more than 20 wells in the south of the Tahe oilfield and were then made into doubly polished thin sections. The thickness of the thin sections is 0.03 mm for petrographic observations. Five O_2yj limestone samples with mesogenetic dissolution were smashed into very small pieces (as small as 1 or 2 mm in size). The eroded and uneroded pieces (Fig. 3a and c) were separated from each other. The separated eroded and uneroded limestone pairs were then crushed into very fine powder in an agate mortar for trace element, including rare earth element (REE), and carbon and oxygen isotope analyses. For purpose of comparison, four lower Ordovician mud-rich limestone hydrocarbon source rocks were also prepared for geochemical analyses.

Whole rock trace elements were analyzed using a Yokogava Analytical Systems PMS-200 Inductively Coupled Plasma-Mass Spectrometry (ICP-MS). For carbon and oxygen isotope analysis, the samples were reacted with 100% pure phosphoric acid and the produced CO_2 was analyzed for isotopic ratios on Mat-252. The $\delta^{18}O$ and $\delta^{13}C$ were reported in permil (‰) relative to the PeeDee Belemnite (VPDB) standard. All the analyses were carried out in the State Key Laboratory for Research of Mineral Deposits (Nanjing University, China). The results of trace element and carbon and oxygen isotope are listed in Tables 1 and 2, respectively.

4. Mesogenetic dissolution of the O_2yj limestone

4.1. Paragenetic festures

The diagenetic events of the limestone in the north uplift area of the Tahe oilfield had been discussed in detail by Chen et al. (2003). In this literature, the diagenetic events that the limestones experienced include: (1) cementation by calcites precipitated in seawater in syngenetic environment, (2) cementation by calcites, compaction and mesogenetic dissolution in burial environment, (3) subaerial karstification because of being uplifted in both middle–late Caledonia and early Hercynian orogenies, and (4) gradual burial.

The paragenetic features of the O_2yj limestone in the south slope area are similar to those of the limestone in the north uplift area except that the limestone in the south slope area was not subaerially exposed. A brief paragenetic sequence includes the following diagenetic events: (1) calcite cementation (Calcite I) in syngenetic seawater environment, (2) calcite cementation (Calcite II) in burial environment, (3) compaction and pressure dissolution resulting in the formation of stylolites, (4) precipitation of euhedral dolomite rhombs along stylolites, and (5) mesogenetic dissolution of limestone matrix, calcite cements and dolomite rhombs.

The Calcite I is generally radial isopachous calcite crust coated around grains in the O_2yj limestone (Fig. 4a). The coating calcite was probably converted from thermodynamically unstable aragonite or magnesium calcite, which was precipitated in syngenetic seawater. The Calcite II is generally blocky coarse calcite filled in the pores between grains (Fig. 4a). As the limestone was buried deeper and deeper, it was compacted and as a result the primary porosity in the limestone got reduced. When the limestone was buried to a depth of as little as about 500 m (Fabricius, 2000), stylolite was commonly developed in the limestone because of pressure dissolution. The stylolite usually cut both grains and two stage calcite cements (Fig. 4c and f). After stylolitisation magnesium-rich formation water migrated along stylolites and as a result euhedral dolomite rhombs formed along some stylolites (Fig. 4g).

4.2. Characteristics of mesogenetic dissolution

Detailed core observations indicate that the mesogenetic dissolution predominately occurred in the O_2yj limestone. Very little or no obvious mesogenetic dissolution was observed in other middle to upper Ordovician formations. The mesogenetic dissolution was generally developed along reticular stylolites, microfractures or bedding planes. Mottled dissolution, dotted dissolution and laminar dissolution are generally present in the well cores (Fig. 3a–c). Even though most of the dissolution pores are very tiny and cannot be observed with the naked eye, there still exist some relatively large pores of about 1 mm or larger (Fig. 3d) where the limestone was severely eroded. The dissolution pores are commonly filled with brown crude oil or dark gray bitumens. Where the limestone is eroded and the dissolution pores are filled with hydrocarbons, the limestone is dark brown; and where the

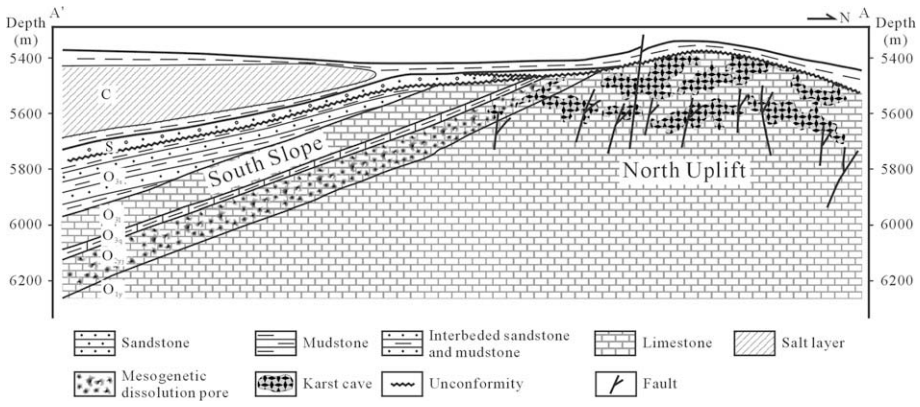

Fig. 2. North–south section of the Tahe oilfield. The section is along the line AA′ in Fig. 1. The reservoir space in the lower Ordovician carbonate of the north uplift is pores and cavities associated with subaerial meteoric dissolution. Comparatively, the reservoir space in O_2yj limestone of the south slope area is predominately mesogenetic dissolution pores.

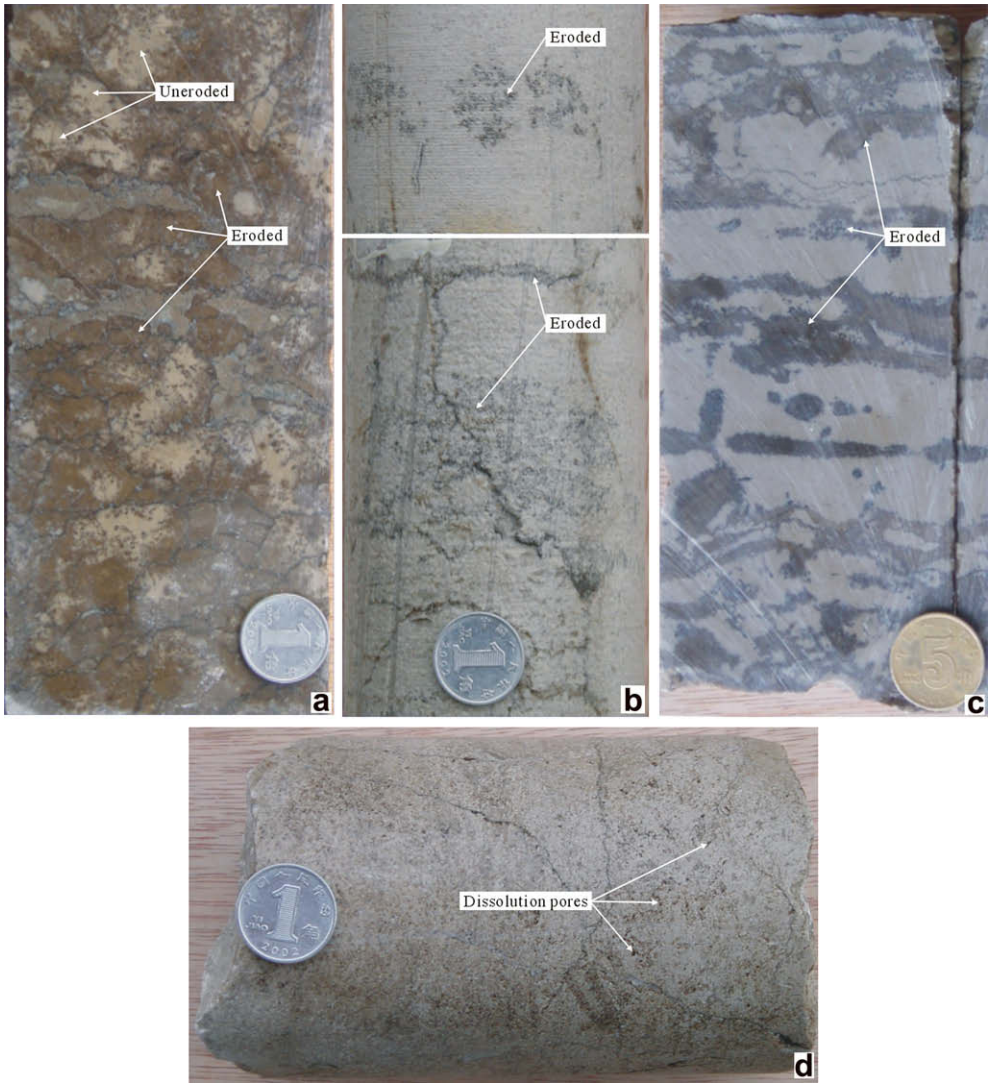

Fig. 3. Characteristics of mesogenetic dissolution present in well cores. (a) Mottled dissolution in O_2yj limestone of well S76, 5580.35 m; (b) dotted dissolution in O_2yj limestone of well S100, 5515.36 m and 5576.30 m, respectively; (c) laminar dissolution in O_2yj limestone of well S67, 5670.74 m; (d) large dissolution pores in O_2yj limestone of well S79, 5588.68 m.

limestone remains uneroded, it is light gray (Fig. 3a). The proportion and extent of mesogenetic dissolution vary greatly from well to well.

Large numbers of tiny dissolution pores charged with crude oil or bitumens can be observed under microscope. The size of dissolution pores is commonly less than 0.1 mm and mostly around 0.01 mm. The grains (Fig. 4b), lime–mud matrix (Fig. 4c) and each stage of calcite cements (Fig. 4d and e) are all eroded to different extents. In the dissolved blocky coarse calcite cements in Fig. 4e, many oil inclusions with light blue fluorescence are also present (Fig. 4f). The dissolution commonly proceeds along stylolites. The calcite cements around stylolites are found remarkably dissolved (Fig. 4d). Some of the dolomite rhombs, as replacement of limestone along stylolites, are also found dissolved (Fig. 4g). The stylolites get rounded and widened because of dissolution (Fig. 4h).

The stylolites and microfractures in limestone can serve as fluid conduits. When moving along such conduits, aggressive fluids will enlarge the conduits and the pre-existing pores as well as create new pores by dissolution, resulting in high dissolution porosity along stylolites or microfractures. The widening of stylolites, the dissolution of dolomite rhombs and blocky calcite cements with oil inclusions demonstrate that the dissolution took place in mesogenetic environment.

The subaerial karstification of limestones in Tahe oilfied is one of the most important events in paragenetic sequences. In general, large caves, karsting breccias, calciferous crust, meniscus or stalagtitic calcite cements and fillings of paleo-soils or silt clasts in caves are the typical phenomena associated with subaerial karstification. Such phenomena had been well documented by boreholes in the north uplift area of Tahe oilfield (Yan, 2002; Huang et al., 2006; Qian et al., 2007; Liu et al., 2007). However, none of these phenomena are found in the O_2yj limestone in the south slope area. In addition, seismic profiles demonstrate that there is no unconformity between the O_2yj limestone and the immediately above stratum and the O_2yj is well bellow the S/O_3 unconformity (Fig. 2). The meteoric alteration generally takes place in depth 0–200 m beneath the unconformity in the Tahe oilfield (Yun et al., 2004; Yan, 2002; Liu et al., 2006), so that the O_2yj limestone in the south slope is out of the scope of the meteoric water. Consequently, the influence of subaerial meteoric karstification on the O_2yj limestone in the south slope area can be ruled out.

As discovered by wells, the mesogenetic dissolution is commonly developed in the O_2yj limestone in south slope area of Tahe oilfield. In the region to the south of O_{2+3} absent line (Fig. 1), the mesogenetic dissolution can be found in cores of almost every well.

Table 1
Results of trace element and rare earth element measurements

Well	S76	S76	S100	S100	S102	S102	T207	T207	S109	S109	T904	T204	T706	S102
Depth (m)	5583.57	5583.57	5617.63	5617.63	6047.4	6047.4	5586.01	5586.01	6250.63	6250.63	5902.65	5995.2	5897.86	6130.54
Formation	O_2yj	O_2yj	O_2yj	O_2yj	O_2yj	O_2yj	O_2yj	O_2yj	O_2yj	O_2yj	O_1	O_1	O_1	O_1
Description	Eroded	Uneroded	Eroded	Uneroded	Eroded	Uneroded	Eroded	Uneroded	Eroded	Uneroded	Mud-rich limestone	Mud-rich limestone	Mud-rich limestone	Mud-rich limestone
Bi	0.0187	0.0020	0.0142	0.0021	0.0093	0.0030	0.0099	0.0040	–	–	0.1729	0.6217	0.3973	0.2363
Ga	0.5466	0.0710	0.4502	0.0818	0.2315	0.0891	0.3282	0.0865	–	–	3.9191	1.8415	2.8803	4.4326
Rb	3.0049	0.5621	3.0799	0.9684	1.7285	0.6118	2.0356	0.7347	–	–	27.0614	9.3171	17.5393	31.6786
Zr	2.9846	0.6804	2.9171	0.6166	1.1658	0.7326	1.9694	0.7555	–	–	17.4173	18.1096	17.7635	18.6572
Nb	0.4785	0.0921	0.3740	0.0844	0.1897	0.0870	0.2863	0.1075	–	–	1.8766	1.8018	1.8392	2.9000
Cs	0.1475	0.0283	0.1580	0.0374	0.0628	0.0303	0.1021	0.0350	–	–	1.1634	0.3988	0.6264	1.3786
Hf	0.0855	0.0218	0.0831	0.0175	0.0370	0.0192	0.0571	0.0175	–	–	0.4340	0.4289	0.4315	0.2864
Ta	0.0334	0.0075	0.0212	0.0044	0.0105	0.0053	0.0126	0.0054	–	–	0.0645	0.0837	0.0741	0.0866
Ti	123.1228	19.3609	102.4865	21.0313	48.3477	24.8753	64.7665	27.6361	–	–	576.0320	564.3182	570.1751	771.6536
V	10.6856	2.7498	8.4875	2.9557	3.5907	2.1333	4.7926	2.6000	–	–	27.5291	45.0286	36.2789	28.0792
Th	0.5710	0.1962	0.3106	0.1188	0.2642	0.1671	0.3221	0.2087	–	–	3.1092	3.7182	2.4150	1.7903
Co	1.0317	0.7261	1.0538	0.6276	1.0231	0.4846	1.5084	0.4941	–	–	4.9933	19.3067	12.1500	5.4872
Pb	1.8431	0.9790	1.2860	0.6665	1.6128	0.8690	2.4613	0.8669	–	–	5.6081	21.7314	13.6698	16.7414
Ba	9.1717	3.7999	10.6605	5.7403	6.6133	6.2052	8.8004	5.6771	–	–	42.7986	100.4362	71.6174	56.5819
Sc	0.6045	0.2862	0.4728	0.2465	0.5348	0.3839	0.4240	0.3503	–	–	2.8348	3.3227	3.0788	4.8019
Y	3.5063	1.8794	3.6622	1.2706	2.4920	2.4473	2.6917	2.2596	–	–	10.0026	20.6088	15.3057	21.2769
Ni	13.2554	7.0131	4.5292	6.0189	12.5233	4.9969	8.7639	5.8653	–	–	23.3195	41.0640	30.1731	26.6190
Mo	1.8513	0.9582	0.6645	0.7988	1.4842	0.6231	0.9377	0.7576	–	–	3.7070	1.3261	2.5166	2.3591
Sr	249.8318	236.3097	144.7122	216.9718	216.8788	253.3190	195.8994	226.8767	–	–	184.4414	181.1790	182.8102	153.1846
U	1.8066	1.1045	0.7518	1.3732	0.9398	0.9477	0.7326	0.9501	–	–	0.6625	0.8670	0.7648	0.7122
Be	0.1430	0.1077	0.2107	0.1255	0.1699	0.2325	0.1467	0.1449	–	–	0.1610	0.1531	0.1571	0.2597
Cr	22.2523	23.6553	16.9178	20.7628	22.8627	21.8775	25.3679	26.4774	–	–	25.8801	36.5455	31.2128	35.3101
Sn	1.9951	2.1853	2.2323	5.4640	2.4808	4.1913	3.6481	3.2268	–	–	3.0193	4.0620	3.5407	3.4586
W	0.6805	0.6357	1.0864	0.3334	0.3850	0.4045	0.4475	1.2203	–	–	0.8478	0.7728	0.8103	1.0993
La	3.1442	1.9964	1.7486	1.5396	2.5049	1.5181	3.2293	2.5682	1.1432	0.8136	21.1405	13.4525	25.1170	16.4816
Ce	4.2323	2.4165	2.0953	1.8103	3.1422	2.0095	4.2234	3.0972	1.4560	1.0935	42.8264	27.7751	45.8531	33.1107
Pr	0.5640	0.3208	0.2542	0.2167	0.3979	0.2569	0.5281	0.4033	0.1593	0.1241	4.0668	2.7325	4.5200	3.4628
Nd	2.7488	1.4170	1.2423	1.0380	1.9065	1.2563	2.5146	1.9049	0.8047	0.5593	19.5400	12.2697	22.3528	14.9422
Sm	0.5046	0.2727	0.2100	0.1910	0.3203	0.2650	0.4791	0.3289	0.1574	0.1044	3.9329	2.2618	4.4381	2.7858
Eu	0.1020	0.0459	0.0569	0.0548	0.0697	0.0489	0.0985	0.0677	0.0343	0.0180	0.8902	0.3596	0.9929	0.5119
Gd	0.4927	0.2896	0.2925	0.2699	0.3467	0.2521	0.5498	0.3822	0.1719	0.0990	4.1695	1.9605	4.9095	2.4793
Tb	0.0777	0.0430	0.0524	0.0440	0.0526	0.0417	0.0850	0.0563	0.0252	0.0132	0.6373	0.2997	0.7095	0.3959
Dy	0.5181	0.2455	0.3367	0.2784	0.3345	0.2292	0.4701	0.2989	0.1400	0.0850	3.6809	1.7084	4.5200	2.2459
Ho	0.1087	0.0566	0.0920	0.0809	0.0690	0.0480	0.1063	0.0713	0.0333	0.0210	0.7256	0.3635	1.0555	0.4870
Er	0.3080	0.1665	0.2702	0.2274	0.1861	0.1315	0.2664	0.1897	0.1030	0.0622	1.8767	1.0283	2.3131	1.3972
Tm	0.0457	0.0253	0.0463	0.0400	0.0262	0.0216	0.0403	0.0306	0.0138	0.0096	0.2834	0.1618	0.3330	0.2124
Yb	0.2707	0.1239	0.2432	0.2144	0.1645	0.1112	0.2391	0.1683	0.0803	0.0431	1.5487	1.0138	1.8635	1.2762
Lu	0.0379	0.0197	0.0439	0.0325	0.0228	0.0141	0.0308	0.0237	0.0103	0.0077	0.2270	0.1523	0.2781	0.1915

Table 2
Results of carbon and oxygen isotope

Well	S76	S76	S100	S100	S102	S102	T207	T207	S109	S109
Depth (m)	5583.57	5583.57	5617.63	5617.63	6047.4	6047.4	5586.01	5586.01	6250.63	6250.63
Formation	O_2yj	O_2yj	O_2yj	O_2yj	O_2yj	O_2yj	O_2yj	O_2yj	O_2yj	O_2yj
Description	Eroded	Uneroded	Eroded	Uneroded	Eroded	Uneroded	Eroded	Uneroded	Eroded	Uneroded
$\delta^{13}C_{PDB}$ (‰)	0.6	1.3	0.5	0.9	0.4	0.8	0.4	0.6	0.3	0.8
$\delta^{18}O_{PDB}$ (‰)	−7.9	−6.4	−7.3	−6.1	−8.1	−6.7	−8.7	−7.6	−8.4	−7

4.3. Influence of mesogenetic dissolution on reservoir physical properties

Reservoir physical properties and oil/gas presence in the O_2yj limestone are directly determined by the extent of mesogenetic dissolution. The S76 well can be employed as a typical example to demonstrate the influence of mesogenetic dissolution. The cores from 5559.2 to 5565.8 m (C-I) of the S76 well belong to the Qiaerbake formation (O_3q), which is immediately above the O_2yj. No mesogenetic dissolution occurs in C-I, and consequently both porosity and permeability are very low. The average porosity and permeability are 0.83% and 0.09×10^{-3} μm^2, respectively. The cores from 5578.0 to 5583.8 m (C-II) and from 5590.2 to 5598.4 m (C-III) belong to the Yijianfang formation. Mesogenetic dissolution of different degrees occurs in both C-II and C-III. In comparison, the dissolution in C-III is much more intensive than that in C-II. There is not any oil/gas presence in C-I (Fig. 5). Comparatively, oil is much more abundance in C-II and C-III. The C-II has oil trace or is stained by oil (Fig. 5). The major part of C-III is saturated with oil (Fig. 5). Only mottled dissolution can be observed in C-II. However, not only mottled dissolution but also millimeter sized dissolution pores can be observed in C-III. The average porosity and permeability of the C-II are 1.35% and 0.28×10^{-3} μm^2, respectively, and those of C-III are 3.69% and 0.57×10^{-3} μm^2, respectively. Based on the porosity and permeability, the reservoir properties of C-III are much better than those of C-II, and C-II is much better than C-I. Generally speaking, the reservoir properties of limestone get better and better with increasing dissolution intensity.

5. Fluid type for mesogenetic dissolution

5.1. Possible fluid types

The fluid that is a potential contributor to the mesogenetic dissolution may be the abundant connate water that is syndepositionally encapsulated in the limestone sediments. However, such fluid is an unlikely agent of mesogenetic dissolution because it quickly comes to chemical equilibrium with surrounding limestone at an early stage of burial diagenesis. In addition, dehydration of evaporite minerals, which occur sporadically in O_2yj limestone, can also provide fluid to the limestone stratum (e.g. Kendall, 1984; Machel and Anderson, 1989). Whereas, such fluid either is not initially unsaturated with respect to calcium carbonate, or if so, it quickly reaches equilibrium when expelled to carbonate host rock. Furthermore, evaporite dehydration operates relatively early during basin subsidence (Hower et al., 1976; Kendall, 1984), generally prior to the development of mesogenetic dissolution porosity.

Organic acids, CO_2 and H_2S are generated during gradual maturation of sedimentary organic matter in the later stages of basin evolution (Tissot and Welte, 1978; Schmidt and McDonald, 1979; Surdam et al., 1982, 1984). The introduction of these acidic substances into subsurface fluid systems alters the chemistry of ambient connate waters, and can make them capable of dissolution (e.g. Spirakis and Heyl, 1988; Moore, 1989; Mazzullo and Harris, 1992). Compared with the fluids generated by the early burial processes previously discussed, the chemically aggressive, undersaturated fluid associated with organic diagenesis is considered to be the most likely agent causing mesogenetic dissolution of limestone.

5.2. Trace element constrains on fluid source

The data of trace elements from Bi to Mn in Table 1 are plotted in Fig. 6, and data of REEs are plotted in Fig. 7. The Fig. 6 demonstrates that the Sr, U, Be, Cr, Sn and W concentration in the eroded and uneroded parts and the source rock is similar, whereas the concentration of other elements, from Bi to Mo, is remarkably different. From Bi to Mo, the concentration of each trace element in the eroded part is intermediate between the uneroded part and source rock, or in other words, is lower than that in the source rock and higher than that in the uneroded part.

As illustrated in Fig. 7, the REE patterns of the source rock and the eroded and uneroded parts of the O_2yj limestone are similar. However, the concentration of REE is different. The REE concentration in the eroded part is slightly higher than that in the uneroded part, but much lower than that in the source rock.

The fluid which contributed to the mesogenetic dissolution should have inherited some signatures, including trace elements, of the fluid source. Through element exchange, diffusion and/or other mechanisms, some compositional signatures of the fluid can partially enter into the eroded limestone during water–rock interaction. Therefore, by measuring element compositions of the eroded limestone, the fluid source can be determined.

Sediments with high organic content are usually enriched in some trace elements. For example, the content of Cu, Cr, Co, Mo, Ni, V and Zn in some black shales is 330 times higher than that in other sediments with no or less organic matter (Brumsack, 1980). The relatively high concentration of these trace elements in the organic-rich sediments can be attributed to (1) the progressive accumulation of trace element in organic tissues, (2) the bacterial sulphate reduction aided by preserved organic matter leading to precipitation of trace element as sulfide, and (3) the adsorption of trace element on clay minerals (Brumsack, 1980; Nijenhuis et al., 1999). The mud-rich dark gray or black carbonate hydrocarbon source rocks of early Ordovician in Tarim basin are similarly also enriched in these trace elements (Fig. 6). The concentration of these trace elements in the source rock is 10–100 times higher than that in the uneroded O_2yj limestone (Fig. 6). The hydrocarbon-bearing fluid derived from such source rock inherited the signatures of high trace element content. And then the trace elements in the fluid can enter into the eroded limestone through element exchange, element diffusion or other mechanisms, resulting in the increasing of Bi to Mo concentration in the eroded limestone. The concentration of Sr to W in source rocks is similar to those in the uneroded limestone, so that the concentration of these trace elements in the eroded limestone is not significantly changed.

As indicated by distributions of trace elements, the fluid responsible for the erosion of limestone can also be similarly inferred to be hydrocarbon-bearing fluid derived from hydrocarbon source rock.

The similar REE patterns between the lower Ordovician mud-rich carbonate hydrocarbon source rock and O_2yj limestone reflect that the two limestone strata were deposited in seawater

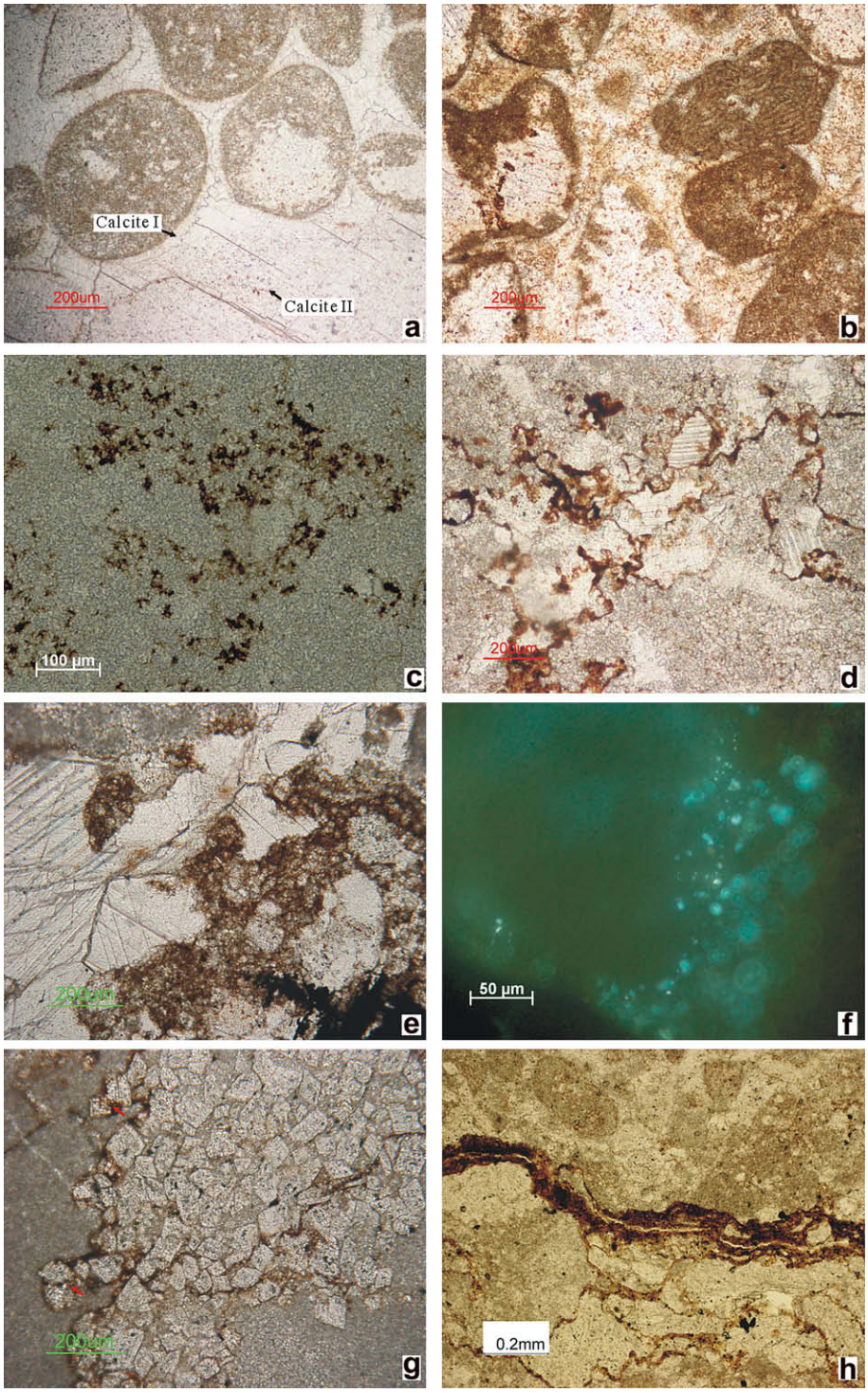

Fig. 4. Mesogenetic dissolution in O_2yj limestone. (a) isopachous calcite crust (Calcite I) around grains and blocky calcite cements (Calcite II) in the pores between grains, the former is related to syngenetic marine water environment and the latter the burial environment, well S99, plane polarized light. (b) Dissolution of both grains and all stages of calcite cements, well S102, 6059.99 m, plane polarized light; (c) dissolution of lime–mud matrix, well S79, 5652.32 m, plane polarized light; (d) dissolution of calcite cements along stylolite, well S102, 6059.87 m, plane polarized light; (e) dissolution of blocky calcite cements precipitated in burial environment, well S109, 6250.36 m, plane polarized light; (f) oil inclusions with light blue fluorescence in blocky calcite cements precipitated in burial environment, well S109, 6250.36 m, ultraviolet light; (g) dissolution of dolomite rhombs (red arrow) precipitated along stylolite, well T702, 5602.37 m, plane polarized light; (h) dissolution along stylolite, well T708, 5809.46 m, plane polarized light.

with similar REE settings, because the REE pattern of carbonates usually inherited that of seawaters (Nothdurft et al., 2004; Wang et al., 1986; Piper, 1991). In seawater, REEs can be adsorbed onto organic matter and clay minerals (Sholkovitz, 1992; Viers et al., 1997), and as a result the concentration of REE in mud- and organic-rich carbonate hydrocarbon source rock is generally much higher than that in other limestones, which contain less or no organic matter.

The concentration of REEs is possibly related to a change of Eh as well. However, in the calcite crystal lattice, the REE elements generally replace Ca^{2+}. All the REEs usually present in the 3+ state, except that europium occurs with a valence of 2+ and cerium

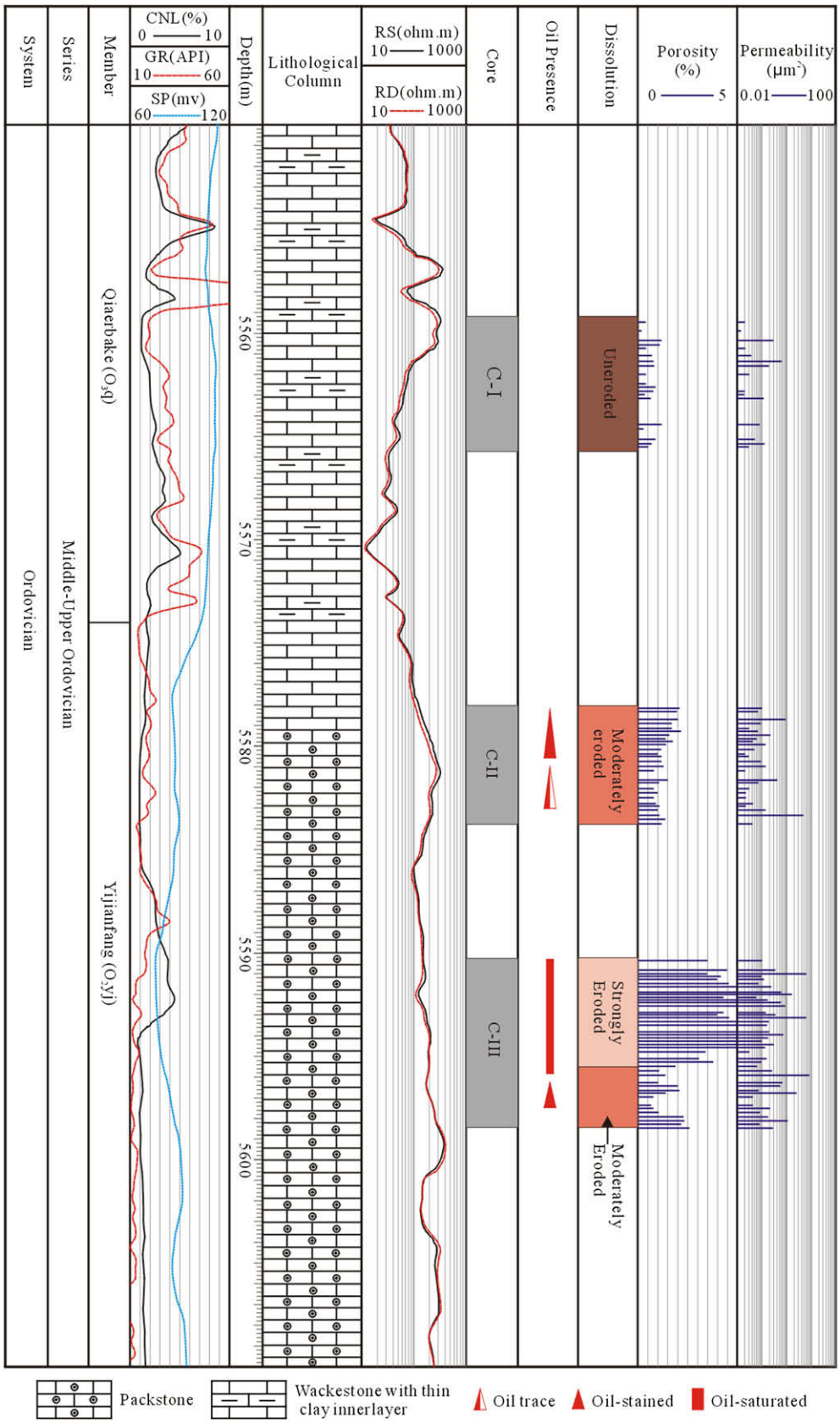

Fig. 5. Petrophysical properties and oil/gas presence in cores with different degree of mesogenetic dissolution in well S76. In well S76, the C-I core was not affected by mesogenetic dissolution, whereas the C-II was moderately eroded and the C-III was strongly eroded. With increasing degree of mesogenetic dissolution from C-I to C-III, the reservoir petrophysical properties and oil/gas content get better and better.

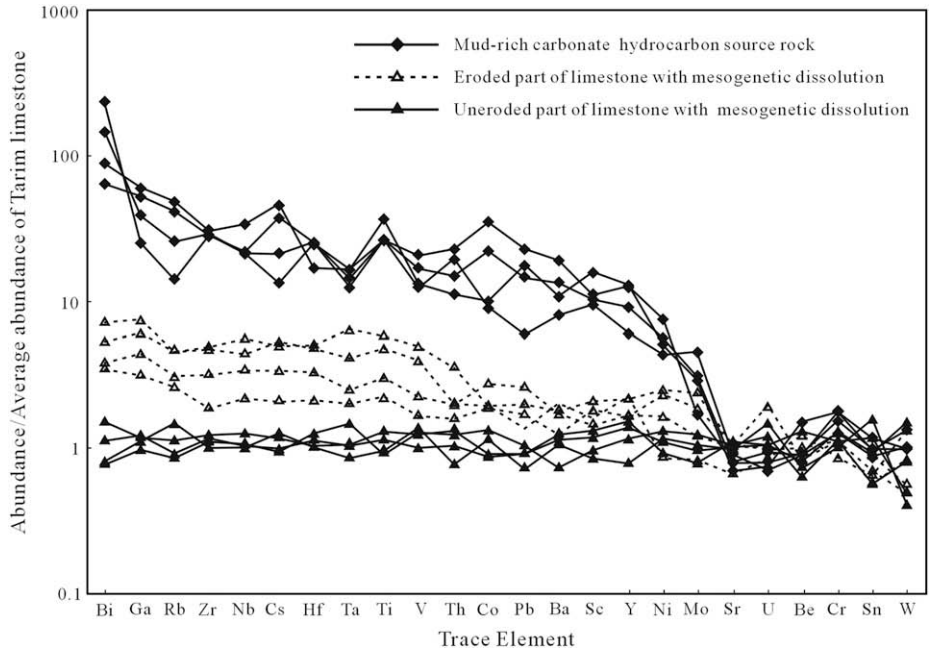

Fig. 6. Trace element distributions of the lower Ordovician mud-rich carbonate hydrocarbon source rock and the eroded and uneroded parts of O_2yj limestone with mesogenetic dissolution.

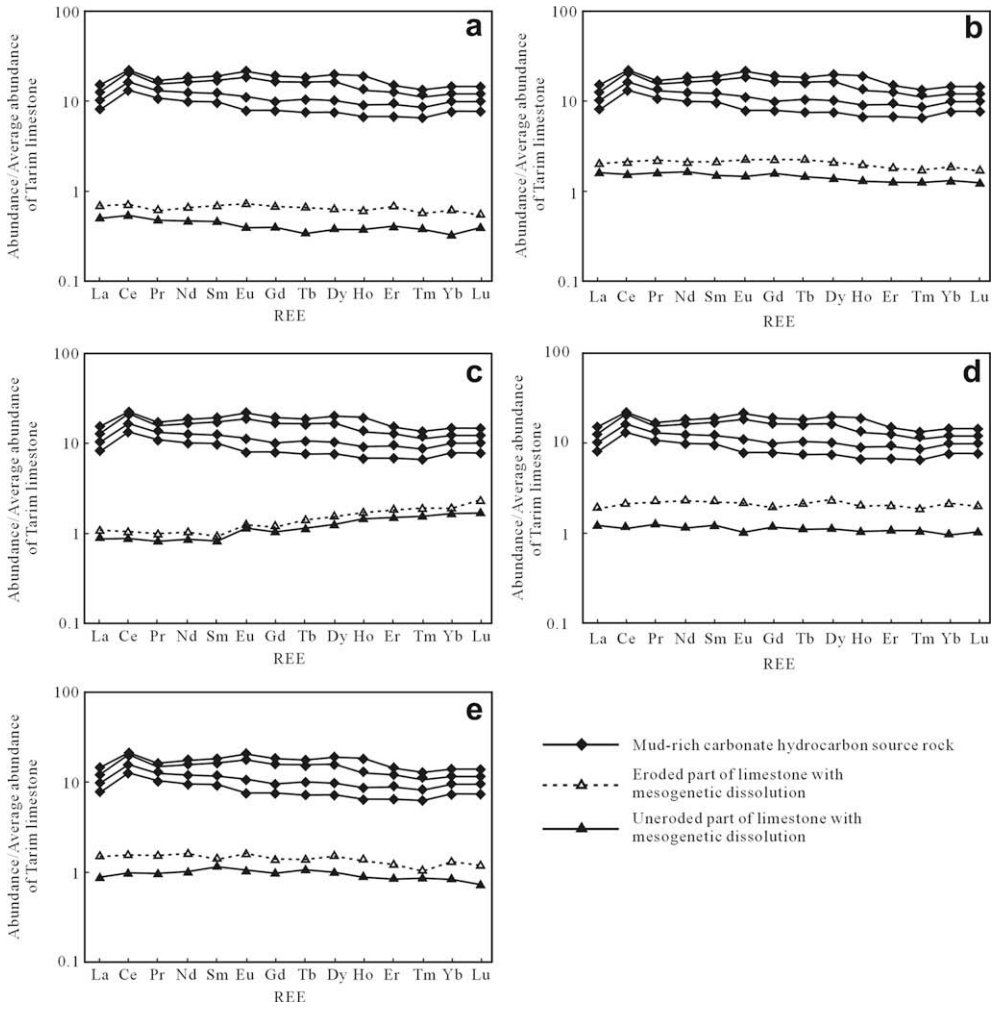

Fig. 7. REE patterns of the lower Ordovician mud-rich carbonate hydrocarbon source rock and the eroded and uneroded parts of O_2yj limestone with mesogenetic dissolution. The REE patterns of the eroded and uneroded pairs of each sample are plotted in one individual chart. The five samples in chart a, b, c, d and e are collected from well S109 (O_2yj, 6250.63 m), T207 (O_2yj, 5586.01 m), S100 (O_2yj, 5617.63 m), S76 (O_2yj, 5583.57 m) and S102 (O_2yj, 6047.40 m), respectively.

a valence of 4+ when the Eh varies. The variation in valence subsequently affects the potential of replacement. So that the change of Eh probably only affects the concentration of Eu and Ce, instead of the whole REE elements.

The measured concentration of REE in the lower Ordovician source rock is 5–15 times higher than that in O_2yj limestone. The acidic materials, such as organic acid, CO_2 and H_2S generated from organic diagenesis, will change the pH condition of the source rock system and thus make the REEs activate (Nesbitt, 1979; Duddy, 1980; Möller and Bau, 1993) and subsequently enter into hydrocarbon-bearing fluid. When migrating into O_2yj limestone, the hydrocarbon-bearing fluid made the REE abundance of eroded part increase through water–rock interaction.

5.3. Carbon and oxygen isotope constrains on fluid type

The $\delta^{13}C_{PDB}$ and $\delta^{18}O_{PDB}$ values of the uneroded part range from 0.6 to 1.3‰ and −7.6 to −6.1‰, respectively (Table 2). The carbon and oxygen isotope compositions are well within the scope of the middle–lower Ordovician limestone in Tarim (Qiao et al., 2001) and well in accordance with the Ordovician limestone worldwide (Veizer et al., 1999). The $\delta^{13}C_{PDB}$ and $\delta^{18}O_{PDB}$ values of the eroded part range from 0.3 to 0.6‰ and −8.7 to −7.3‰, respectively (Table 2).

Although the carbon and oxygen isotope compositions of the eroded part are also within the scope of the Ordovician carbonates, they are uniformly slightly lighter than the uneroded part. The CO_2 of organic origin is generally relatively light in carbon isotope composition, and the hydrocarbon-bearing fluid usually contains large amount of CO_2/HCO_3^- of organic origin. Altered by the hydrocarbon-bearing fluid, the eroded part would be slightly lighter in carbon isotope composition. The mesogenetic dissolution generally took place when limestone was buried to a certain depth, at which the temperature of the hydrocarbon-bearing fluid is relatively high. The reason for the lighter oxygen composition of the eroded part is that the water–rock interaction took place at relatively high temperature.

5.4. Fluid type for mesogenetic dissolution

The different trace element and carbon and oxygen isotopic fingerprints between the eroded and uneroded O_2yj limestone are doubtlessly the result from erosion of limestone by a certain type of eroding fluid. Trace element and stable isotope results demonstrate that the eroding fluid responsible for the mesogenetic dissolution is hydrocarbon-bearing fluid originated from carbonate hydrocarbon source rocks, consistent with what Mazzullo and Harris (1992) had theoretically concluded. The lower Ordovician hydrocarbon source rocks in Tabei uplift and adjacent depressions, such as Manjiaer and Caohu depressions, have experienced multi-stage evolution and have the ability to provide sufficient hydrocarbons. When hydrocarbons, which contain organic acids, CO_2 and H_2S, migrate into the overlaying O_2yj limestone, the limestone is subsequently eroded.

6. Conclusion

The mesogenetic dissolution developed in the O_2yj limestone is greatly significant for the limestone reservoirs in the south slope area of the Tahe oilfield. The mesogenetic dissolution occurs as mottled, dotted and laminar dissolution presented in well cores. The limestone grains, lime–mud matrix, all stages of calcite cements and dolomite rhombs precipitated along stylolites are all eroded. Trace element and carbon and oxygen isotope analyses prove that the fluid responsible for mesogenetic dissolution is hydrocarbon-bearing fluid originated from hydrocarbon source rocks.

References

Brumsack, H.J., 1980. Geochemistry of Cretaceous black shales from the Atlantic Ocean (DSDP Legs 11, 14, 36 and 41). Chemical Geology 31, 1–25.

Chen, Q.L., Qian, Y.X., Ma, H.Q., Wang, S.Y., 2003. Diagenesis and porosity evolution of the Ordovician carbonate rocks in Tahe oilfield, Tarim basin. Petroleum Geology and Experiment 25 (6), 729–734 (in Chinese with English abstract).

Duddy, L.R., 1980. Redistribution and fractionation of rare earth and other element in a weathered profile. Chemical Geology 30, 363–381.

Fabricius, I.L., 2000. Interpretation of burial history and rebound from loading experiments and occurrence of microstylolites in mixed sediments of Caribbean Sites 999 and 1001. In: Leckie, R.M., Sigurdson, H., Acton, G.D., Draper, G. (Eds.), Proceedings of the Ocean Drilling Program: Scientific Results, 165, pp. 177–190.

Fan, P., Zhang, B.S., Wang, Y.X., Ying, G.G., Zhang, J., 1991. Oil and gas geochemistry. In: Fan, P., Ma, B. (Eds.), Petroleum Geology of Tarim. Science Press, Beijing, pp. 1–72.

Graham, S.A., Brassell, S., Carroll, A.R., et al., 1990. Characteristics of selected petroleum source rocks, Xianjiang Uygur autonomous region, Northwest China. AAPG Bulletin 74, 493–512.

Halley, R.B., Schmoker, J.W., 1983. High porosity Cenozoic carbonate rocks of south Florida: progressive lose of porosity with depth. AAPG Bulletin 67, 191–200.

Hendrix, M.S., Brassell, A.C., Carroll, A.R., Graham, S.A., 1995. Sedimentology, organic geochemistry, and petroleum potential of Jurassic coal measures: Tarim, Junggar, and Turpan basins, northwest China. AAPG Bulletin 79, 929–959.

Heydari, E., 1997. Hydrotectonic models of burin diagenesis in platform carbonates based on formation water geochemistry in North American sedimentary basins. In: Montanez, I.P., Gregg, J.M., Shelton, K.L. (Eds.), Basin-wide Diagenetic Patterns: Integrated Petrologic, Geochemical, and Hydrologic Considerations. SEPM Special Publication, No. 57, pp. 53–79.

Hower, J., Eslinger, E.V., Hower, M.E., Perry, E.A., 1976. Mechanism of burial and metamorphism of argillaceous sediment: 1. Mineralogical and chemical evidence. Geological Society of America Bulletin 87, 725–737.

Huang, C.Y., Zou, S.Z., Pan, W.Q., Xia, R.Y., Liu, J.J., Tiang, J.S., 2006. Structure pattern of rift-cavity oil gas pool in carbonate rock under moisture paleo-environment – a case study on the Ordovician in Tarim basin. Carsologica Sinica 25 (3), 250–255 (in Chinese with English abstract).

James, N., Choquette, P.W., 1984. Diagenesis 9 – limestones, the meteoric diagenetic environment. Geoscience Canada 11, 161–194.

Jia, Z.Y., Hao, S.S., 1989. Formation and Distribution of Oil and Gas in Carbonates. Petroleum Industry Press, Beijing (in Chinese).

Kang, Y.Z., Kang, Z.H., 1996. Tectonic evolution and oil and gas of Tarim Basin. Journal of Southeast Asian Earth Sciences 13, 17–325.

Kendall, A.C., 1984. Evaporites. In: Walker, R.G. (Ed.), Facies Models: Geochemical Canada. Reprint Series, 1, pp. 259–298.

Lee, K.Y., 1985. Geology of the Tarim Basin with Special Emphasis on Petroleum Deposits, Xinjiang Uygur Zishiqu, Northwest China. US Geological Survey Open-File Report 85–0616.

Liu, C.Y., Wu, M.B., Gong, G., 2006. Caledonian kar stification of Ordovician carbonates in the Tahe oilfield, northern Tarim basin, Northwest China, and its petroleum geological significance. Geological Bulletin of China 25 (9–10), 1128–1134 (in Chinese with English abstract).

Liu, X.P., Sun, D.S., Wu, X.S., 2007. Ordovician paleo-karst landform and its control on reservoirs in west Lungu region, Tarim basin. Petroleum Geology and Experiment 29 (3), 265–268 (in Chinese with English abstract).

Liu, X.Z., 1997. Studies on Carbonate Reservoir in Center of Tarim Basin. Research Report of Managing Department for Petroleum E&P of Tarim Basin (Kuerle), p. 35 (in Chinese).

Machel, H.G., Anderson, J.H., 1989. Pervasive subserface dolomitization of the Nisku Formation in central Alberta. Journal of Sedimentary Petrology 59, 891–911.

Mazzullo, S.J., Harris, P.M., 1992. Mesogenetic dissolution: its role in porosity development in carbonate reservoir. AAPG Bulletin 76 (5), 607–620.

Möller, P., Bau, M., 1993. Rare-earth patterns with positive cerium anomaly in alkaline waters from Lake Van, Turkey. Earth and Planetary Science Letters 117, 671–676.

Moore, C.H., 1989. Carbonate Diagenesis and Porosity, Developments in Sedimentology. Elservier, Amsterdam, p. 46, 338 pp.

Nesbitt, H.W., 1979. Mobility and fractionation of rare earth elements during weathering of a granodiorite. Nature 279, 206–210.

Nijenhuis, I.A., Bosch, H.J., Sinnighe Damsté, J.S., Brumsack, H.J., de Lange, G.J., 1999. Organic matter and trace element rich sapropels and black shales: a geochemical comparison. Earth and Planetary Science Letters 169, 277–290.

Nothdurft, L.D., Webb, G.E., Kamber, B.S., 2004. Rare earth element geochemistry of Late Devonian reefal carbonates, Canning Basin, Western Australian: conformation of seawater REE proxy in ancient limestones. Geochimica et Cosmochimica Acta 68 (2), 263–283.

Piper, D.Z., 1991. Geochemistry of a Tertiary sedimentary phosphate deposit, Baja California Sur, Mexico. Chemical Geology 92, 283–316.

Qian, Y.X., Chen, Y., Chen, Q.L., You, D.H., Chu, S.L., 2006. General characteristics of burial dissolution for Ordovician carbonate reservoirs in the northwest of Tazhong aera. Acta Petrolei Sinica 27, 47–52 (in Chinese with English abstract).

Qian, Y.X., Taberner, C., Chu, S.L., D.H., Wang, R.Y., 2007. Diagenesis comparison between epigenetic karstification and burial dissolution in carbonate reservoirs – an instance of Ordovician carbonate reservoirs in Tahe and Tazhong regions, Tarim basin. Marine Petroleum Geology 12 (2), 1–7 (in Chinese with English abstract).

Qiao, G.S., Zhang, R.H., Chen, D.Z., Zhu, J.Q., Jiang, M.S., 2001. Carbon and strontium isotope variations and responses tosea-level fluctuations in the Ordovician of the Tarim Basin. Science in China, Ser. D 44 (9), 816–823.

Schmidt, V., McDonald, D.A., 1979. The role of secondary porosity in the course of sandstone diagenesis. SEMP Special Publication 26, 175–207.

Sholkovitz, E.R., 1992. Chemical evolution of rare earth elements: fractionation between colloidal and solution phases of filtered river water. Earth Planetary Science Letters 114, 77–84.

Scholle, P.A., 1977. Chalk diagenesis and its relationship to petroleum exploration: oil from chalks, a modern miracle. AAPG Bulletin 61, 982–1009.

Scholle, P.A., Halley, R.B., 1985. Burial diagenesis: out of sight, out of mind!. In: Schneidermann, N., Harris, P.M. (Eds.), Carbonate Cements. EPSM Special Publication, 36, pp. 309–334.

Spirakis, C.S., Heyl, A.V., 1988. Possible effects of thermal degradation of organic matter on carbonate paragenesis and fluorite precipitation in Mississippi Valley-type deposits. Geology 16, 1117–1120.

Surdam, R.C., Boese, S.W., Crossey, L.J., 1982. Role of organic and inorganic reactions in development of secondary porosity in sandstones (abs.). AAPG Bulletin 66, p. 635.

Surdam, R.C., Boese, S.W., Crossey, L.J., 1984. The chemistry of secondary porosity. In: McDonald, D.A., Suedan, R.C. (Eds.), Clastic Diagenesis. AAPG Memoir, 37, pp. 127–149.

Tissot, B.P., Welte, D.H., 1978. Petroleum formation and occurrence: a new approach to oil and gas exploration. Springer-Verlag, New York, 538 pp.

Tong, X.G., 1992. The Tectonic Geological Characters and Distribution Pattern of Hydrocarbon Resources in Tarim Basin, Petroleum Exploration Works of the Tarim Basin. Xinjiang Science and Technology Press, Wulumuqi, pp. 17–22 (in Chinese).

Viers, J., DupréB, B., Polvé, M., Schott, J., Dandurand, J.L., Braun, J.J., 1997. Chemical weathering in the drainage basin of a tropical watershed (Nsimi-Zoetele site, Cameroon): comparison between organic-poor and organic-rich waters. Chemical Geology 140, 181–206.

Veizer, J., Ala, D., Azmy, K., Bruckschen, P., Buhl, D., Bruhn, F., Carden, G., Diener, A., Ebneth, S., Godderis, Y., Jasper, T., Korte, C., Pawellek, F., Podlaha, O., Strauss, H., 1999. $^{87}Sr/^{86}Sr$, $\delta^{13}C$ and $\delta^{18}O$ evolution of Phanerozoic seawater. Chemical Geology 161, 59–88.

Wang, Q., Nishidai, T., Coward, M.P., 1992. The Tarim basin, NW China, formation and aspects of petroleum geology. Journal of Petroleum Geology 15, 5–34.

Wang, S.Y., Chen, Q.L., Ma, H.Q., 2003. Burial corrosion of lower Ordovician carbonate rocks and its influence on reservoirs in Tahe oilfield, Tarim basin. Petroleum Geology and Experiment 25, 557–561 (in Chinese with English abstract).

Wang, Y.L., Liu, Y.G., Schmitt, R.A., 1986. Rare earth geochemistry of South Atlantic deep sediments, Ce anomaly change at 54 Ma. Geochemica et Cosmochimica Acta 50, 1337–1355.

Wei, G.Q., Jia, C.Z., Song, H.Z., Shi, Y.S., Lu, H.F., Li, Y.H., 2000. Ordovician structure-depositional model and prediction of profitable crack reservoir of carbonate rock in Tazhong area, Tarim Basin. Acta Sedimentary Sinica 18, 408–413 (in Chinese).

Yan, X.B., 2002. Characteristics of paleo-karst and reservoir in the lower Ordovician of Tahe oilfield. Journal of Jianghan Petroleum Institute 24 (12), 23–25 (in Chinese with English abstract).

Ye, D.S., Wang, S.Y., Zhang, X.M., 1994. Sedimentation, Diagenesis and Reservoir Evolution of Carbonates in the North of Tarim Basin. Chengdu University of Science and Technology Press, Chengdu. pp.70–77.

Yu, L.R., Fu, H., 2006. Influence of tectonic movement on Ordovician carbonates of Tahe oilfield: Nature Gas Exploration and Development 29 (2), 1–6 (in Chinese with English abstract).

Yun, L., Xiao, Z.G., Xu, M.J., 2004. A brief talk on gas exploration potential in the platform basin region, Tarim basin. Oil and Gas Geology 25 (4), 428–432 (in Chinese with English abstract).

Yung, T.S., Liu, W.C., 1992. Palaeographic evolution and sedimentary history in Palaeozoic in the Tarim Basin. In: Tang, X.G., Liang, D.G. (Eds.), Paper Compilation of Oil and Gas Formation in the Tarim Basin. Xinjiang Sciences and Sanitation Press, Wulumuqi, pp. 103–106 (in Chinese).

Zenger, D.H., Junham, J.B., Ethington, R.L., 1980. Concepts and models of dolomitization. SEPM Special Publication 28, 320 pp.

Zhang, S.C., Hanson, A.D., Moldowan, J.M., Grahm, S.A., Liang, D.G., Chang, E., Fago, F., 2000. Paleozoic oil-source rock correlations in the Tarim basin, NW China. Organic Geochemistry 31, 273–286.

Zhang, T., Yan, X.B., Wang, S.Y., Yu, M.S., 2004. Characteristics and genesis of reef-bank facies reservoirs with dissolution pores in Ordovician Yijianfang formations in Tahe Oilfield. Oil and Gas Geology 25, 462–471 (in Chinese with English abstract).

Zhang, Z.M., 1992. A preliminary investigation of the strata system and the tectonic evolution of the central uplift in the Tarim Basin. In: Tang, X.G., Liang, D.G. (Eds.), Paper Compilation of Oil and Gas Formation in the Tarim Basin. Xinjiang Sciences and Sanitation Press, Wulumuqi, pp. 100–103 (in Chinese).

Zhou, Q.J., Zheng, J.J., 1990. Tectonic Characters of the Tarim Basin. Science Press, Beijing, pp. 18–28 (in Chinese).